Transcription coactivator OCA-B/Pou2af1 is sufficient to promote T cell-intrinsic CD4 memory and prospectively identifies memory precursors

Authors: Wenxiang Sun[1,2,†], Erik P. Hughes[1,2,†], Heejoo Kim[1,2,†], Jelena Perovanovic[1,2], Krystal R. Charley[1,2], Junhong Du[1,2], Andrea Ibarra[1,2], J. Scott Hale[1], Matthew A. Williams[1,2], Dean Tantin[1,2,3,*]

[1]Department of Pathology, University of Utah School of Medicine, Salt Lake City, UT 84112, U.S.A.
[2]Huntsman Cancer Institute, University of Utah School of Medicine, Salt Lake City, UT 84112, U.S.A.
[3]Lead contact
[*]Correspondence to Dean Tantin: dean.tantin@path.utah.edu

[†]Equal contributors
W. Sun's current affiliation is Sumitomo Pharma Oncology, 3900 N. Traverse Mountain Blvd., Suite 100, Lehi, Utah 84043
H. Kim's current affiliation is Janssen Research & Development, LLC., Neuroimmunology Drug Discovery, 3210 Merryfield Row, San Diego, CA 92121.
J. Perovanovic's current affiliation is Recursion Pharmaceuticals, 41 400 W, Salt Lake City, UT 84101

Characters in title (including spaces): 128
Words in abstract: 142
Characters in manuscript (no spaces, excluding legends, methods, references): 19,921
Total main figures and tables: 5

The molecular mechanisms leading to the establishment of immunological memory are inadequately understood, limiting the development of effective vaccines and durable anti-tumor immune therapies. Here we show that ectopic OCA-B expression is sufficient to drive T cells towards a memory fate, while having minimal effects on primary antiviral effector response. At primary effector response, short lived effector T cell compartments are expanded but show increased expression of *Gadd45b* and *Socs2*, while memory precursor effector cell clusters show increased expression of *Bcl2*, *Il7r*, *Tcf7* and *Slamf6*, consistent with increased memory potential. Using an OCA-B mCherry reporter mouse allele, we observe high reporter expression in $CD4^+$ T_{CM} cells. We show that endogenously elevated OCA-B expression prospectively identifies memory precursor cells with increased survival capability and memory recall potential. Cumulatively, the results demonstrate that OCA-B is necessary and sufficient to promote CD4 T cell memory in vivo.

Introduction

The ability to respond robustly to secondary antigen exposures (immune memory) is a defining feature of the adaptive immune system and forms the physiologic basis for vaccination (Sallusto et al., 2010). Immune memory can also drive autoimmune and antitumor responses (Cafri et al., 2019; Gearty et al., 2022; Rosato et al., 2019; Schnell et al., 2021). Strategies that promote memory have the potential to improve both vaccine efficacy and tumor immunotherapy. Central memory T cells (T_{CM}), which home to secondary lymphoid organs, are particularly long lived and demonstrate high proliferative capacity upon stimulation.

Multiple transcription factors and epigenetic regulators are known to modulate formation or function of T_{CM}, including Blimp1 (Kallies et al., 2009; Rutishauser et al., 2009; Shin et al., 2013), Suv39h1 (Pace et al., 2018), T-bet (Joshi et al., 2007; Marshall et al., 2011), Foxo1 (Hess Michelini et al., 2013; Rao et al., 2012), Bcl6 (Ichii et al., 2007; Pepper et al., 2011), Eomes (Banerjee et al., 2010) and TCF1 (Utzschneider et al., 2016). Many of these factors manifest pro-memory functions more clearly in $CD8^+$ compared to $CD4^+$ T cells, where the molecular basis of memory is more poorly defined. In $CD4^+$ T cells, the lymphocyte-restricted transcriptional coregulator OCA-B (also known as OBF-1 and Pou2af1) is induced upon T cell antigen stimulation (Sauter and Matthias, 1997; Zwilling et al., 1997). Germline OCA-B deletion results in normal primary T cell responses to LCMV, but attenuates $CD4^+$ memory T cell formation and recall response. Elevated *Ocab* (*Pou2af1*) mRNA levels are seen in $CD4^+CD25^{lo}$ early effector cells that are enriched for memory potential (Snook et al., 2018). OCA-B is also associated with autoimmunity (Ban et al., 2006; Chevrier et al., 2014; Kim et al., 2021; Nakamura et al., 2012).

Here, we show that OCA-B deletion in T cells selectively reduces memory responses. We show that ectopic OCA-B expression does not alter effector cell numbers at peak T cell response to LCMV, but is sufficient to expand the memory recall effector pool at the expense of empty vector-transduced controls. The effect becomes progressively stronger at later timepoints. mRNA expression profiling of effector cells ectopically expressing OCA-B reveals gene expression changes associated with effector and memory properties, signaling and homing. These include global increases in *Socs2* and *Gadd45b*, expansion of short-lived terminal effector T cell populations, and increases in *Tcf7* and *Il7r* in specific memory precursor populations. Using an OCA-B reporter mouse, we show that elevated levels of endogenous OCA-B in effector T cells during the primary response prospectively identifies $CD4^+$ T effector cells with enhanced survival and expansion capability following viral rechallenge.

Results and Discussion

71 **OCA-B in T cells is required for robust CD4$^+$ T cells memory recall responses**
72 We used a conditional *Ocab* (*Pou2af1*) mouse allele crossed to a CD4-Cre driver, which efficiently
73 deletes OCA-B in T cells (Kim et al., 2021), to study effects of T cell-specific OCA-B loss. We
74 infected *Ocab*$^{fl/fl}$;CD4-Cre and control *Ocab*$^{fl/fl}$ mice with LCMV^{Arm} and measured specific T cell
75 responses using I-A^b/gp$_{66–77}$ tetramer staining. No significant differences in the frequency of positive
76 cells were observed at 8 days post-primary infection (dpi, Fig. S1 A). Rechallenging these mice with
77 *Listeria monocytogenes* expressing the LCMV glycoprotein epitope (Lm-gp61) (Shen et al., 1995)
78 elicited a trending but nonsignificant decrease in the frequency of CD4$^+$ I-A^b/gp$_{66–77}$$^+$ CD4$^+$ T cells
79 undergoing memory recall response in *Ocab*$^{fl/fl}$;CD4-Cre mice (Fig. 1A, D40+7). The responding cells
80 showed little change in IL-2/IFNγ double-producing CD4$^+$ T cells, but a significant decrease in IFNγ
81 single-producers (Fig. S1 B, C). The same cells showed minimal changes in ICOS, PD-1, Ly6C or
82 CD62L expression (Fig. S1 D). These results indicate that infection of T cell-conditional OCA-B
83 knockout mice with LCMV results in deficiencies in memory recall response IFNγ expression.
84 The relatively small reductions in frequencies of tetramer$^+$ CD4$^+$ T cells at recall response may
85 reflect selection for a small percentage of cells escaping OCA-B deletion. This selection can be
86 circumvented using bone marrow chimeras in which conditional deficient or control cells are competed
87 against wild-type T cells in the same mice. We generated bone marrow radiation chimeras in which
88 wild-type donors were co-engrafted with congenically-marked *Ocab*$^{fl/fl}$;CD4-Cre or control *Ocab*$^{fl/fl}$
89 cells in the same recipients. After 8 weeks to allow engraftment, recipient mice were infected with
90 LCMV. The ratio of antigen-reactive *Ocab*$^{fl/fl}$ control effector CD4$^+$ T cells to wild-type competitor
91 was close to 1:1 at 8 dpi. OCA-B deficient (*Ocab*$^{fl/fl}$;CD4-Cre) cells were slightly reduced relative to
92 wild-type competitor (Fig. S1 E). To investigate the effects of T cell-specific OCA-B loss on memory
93 recall responses, we rechallenged mice with Lm-gp61. Following rechallenge, the control to wild-type
94 cell ratio remained close to 1:1 at both primary and memory recall response, while wild-type
95 competitor cells were greatly increased at the expense of OCA-B deficient cells specifically at recall.
96 (>8-fold, Fig. S1 E, F). These findings indicate that, similar to T cell-conditional Oct1 deficiency and
97 global OCA-B deficiency (Shakya et al., 2015), T cell-conditional OCA-B deficiency in bone marrow
98 chimeras results in severe and selective deficiencies in CD4$^+$ T cell memory recall responses.
99
100 **Ectopic OCA-B expression is sufficient to enhance CD4$^+$ T cell memory responses in vivo**
101 We transduced Thy1.1$^+$ SMARTA TCR transgenic donor T cells with an MSCV vector expressing
102 mouse OCA-B. In parallel, Ly5.1$^+$ (CD45.1$^+$) control SMARTA cells were transduced with empty

103 vector (EV). SMARTA mice express a transgenic TCR recognizing an immunodominant LCMV
104 glycoprotein ($GP_{61–80}$) $CD4^+$ epitope (Oxenius et al., 1998). The cells were mixed 1:1 and adoptively
105 co-transferred into $Thy1.2^+Ly5.2^+$ recipients as depicted in Fig. 1 A. Fibroblasts, which express no
106 endogenous OCA-B, efficiently express OCA-B protein when transduced with pMIG-OCA-B (Fig. 1
107 B). After transfer, recipient mice were infected with LCMV and the cell populations were detected by
108 flow cytometry using GFP expressed from MSCV and congenic markers from the donor T cells. The
109 host T cells mounted normal responses to LCMV, allowing SMARTA cells to be monitored in the
110 context of a normal host response. At 8 dpi, effector EV and OCA-B transduced cells expanded
111 equivalently, maintaining the same ratio in both spleen and peripheral blood (Fig. 1 C and D). Another
112 group of mice were infected with LCMV and allowed to clear the virus and form memory. Recall
113 responses were induced by re-challenge using Lm-gp61. At peak T cell response to rechallenge (52+7
114 and 110+7 dpi), ~50-fold more OCA-B overexpressing SMARTA cells were present (Fig. 1 C and D).
115 Ratios of percentages from multiple mice are quantified in Fig. 1 E. These results indicate that OCA-B
116 expression enhances the ability of $CD4^+$ T cells to induce memory responses.
117 At 8 dpi, GFP^+ SMARTA effector T cells were uniformly $CD44^{hi}CD62L^{lo}$ with few changes
118 induced by ectopic OCA-B expression (Fig. 1 F). ICOS and PD-1 levels were slightly diminished by
119 OCA-B overexpression. Ly6C was not significantly altered (Fig. 1 F and G). To investigate if ectopic
120 OCA-B expression induces gene expression changes in effector cells that promote later memory
121 formation, we profiled gene expression using splenic SMARTA T cells at 8 dpi. $CD4^+$ cells were first
122 isolated by magnetic isolation, then $Ly5.1+/5.2^+$ and GFP^+ cells were further isolated by FACS. We
123 identified ~600 down-regulated genes and ~200 up-regulated genes (Table S1). Unsupervised
124 hierarchical clustering identified differentially expressed gene clusters (Fig. 2 A). Down-regulated
125 genes included *Sell*, which encodes CD62L, and genes specific to alternative $CD4^+$ lineages, such as
126 *Bcl6* and *Foxp3*. The top up-regulated gene, *Pou2af1*, encodes OCA-B, providing a quality control.
127 Other up-regulated genes were associated with effector activity (*Tbx21*, *Zeb2*), exhaustion
128 (*Ikzf2*/*Helios*) and attenuation of T cell signaling and proliferation (*Socs2*, *Gadd45b*). *Gadd45b*
129 promotes autoimmune disease and anti-tumor immune responses (Ju et al., 2009; Liu et al., 2005; Luo
130 et al., 2011; Rodriguez-Jimenez et al., 2021). Gene ontology (GO) analysis of the up-regulated genes
131 identified terms associated with H3K9me3 regulation. Down-regulated genes by contrast were strongly
132 associated with H3K27me3 in $CD4^+$ and $CD8^+$ memory T cells (Fig. 2 C). ChIP-X Enrichment
133 Analysis (ChEA) (Lachmann et al., 2010) identifies Tp53 and Smc3 as factors that also regulate the
134 gene set induced by OCA-B ectopic expression (Fig. 2 D). p53 and SMC3 may therefore also control
135 expression of these genes alongside OCA-B, or could themselves be controlled by OCA-B to mediate

136 gene induction via an indirect mechanism. Sets of significant Molecular Function, Epigenomic
137 Roadmap and ChEA GO terms are shown in Table S2. These changes may be sufficient to confer
138 potential increased memory formation, as small advantages compounded over time can result in the
139 large observed effects.

140 Two other genes associated with T cell survival and memory formation, *Il7r* and *Tcf7* (Joshi et
141 al., 2007; Utzschneider et al., 2016), were counterintuitively decreased in bulk RNA-seq. *Il7r* for
142 example encodes a cytokine receptor important for T cell survival. Effector $CD4^+$ T cell populations
143 are heterogeneous, with memory progenitor cells comprising a small proportion of the effector T cell
144 population (Blattman et al., 2002; Joshi et al., 2007; Snook et al., 2018). Increased *Il7r* expression in
145 memory progenitors may be obscured in bulk RNA-seq by decreases in the larger populations of
146 terminal effector cells, which may lead to more culling to create greater capacity for memory. We
147 therefore also performed single-cell RNA-sequencing (scRNA-seq) at D8 post-LCMV infection.
148 Uniform manifold approximation and projection (UMAP) using EV-transduced cells revealed a variety
149 of populations (Fig. 3 A, Table S3). Clusters 1 and 4 were enriched for genes such as *Ccr7*, *Bcl2*,
150 *Slamf6* and *Tcf7* (both clusters), *Tox* (cluster 1), and *Cxcr5*, *Il7r*, *Icos* and *Cd69* (cluster 4, Table S3).
151 These clusters likely contain memory precursors. "T Memory Cells" was identified as the top cluster 4
152 term (Fig. 3 A). Clusters 0, 2 and 6 by contrast were enriched in *Ccl5*, *Ifng* and *Tbx21*, respectively
153 (Table S3), and likely comprise terminal effectors. Cluster 5 was enriched for genes encoding histones,
154 cyclin-dependent kinases and proliferating cell nuclear antigen (PCNA) and likely represent
155 proliferating effectors. OCA-B-transduction resulted in more uniform clustering with fewer and more
156 tightly spaced clusters identified using the same parameters (Fig. 3 B). Cluster 0 contained the largest
157 number of cells and was marked by *Zeb2*, *Klrg1* and *Tbx21* (Table S3). Clusters 1 and 2 were also
158 associated with effector activity. One difference between the empty vector- vs. OCA-B-transduced
159 effector cell clusters was the selective expression of *Socs2*, which encodes an attenuator of T cell
160 signal transduction, more robustly in the OCA-B-transduced condition (Fig. 3 C). These results suggest
161 an expansion of short-lived effector cells in the OCA-B-transduced condition.

162 OCA-B transduced cluster 3 was associated with effector/memory progenitor activity (Fig. 3).
163 Interestingly, *Ikzf2*, which has been associated with $CD4^+$ T cell exhaustion (Crawford et al., 2014),
164 was not enriched in the memory-associated cluster 3 but was enriched in the equivalent cluster 4 in
165 EV-transduced cells (Table S3). Several memory-associated genes in the memory progenitor OCA-B-
166 expressing cluster 3 were increased compared to equivalent memory progenitor EV-transduced
167 clusters. *Tcf7* was increased by >4-fold in OCA-B cluster 3, but only 2-fold in empty vector clusters 1
168 and 4 (Table S3). *Slamf6* was increased by >3-fold in OCA-B cluster 3, but <2.5-fold in empty vector

169 clusters 1 and 4. *Bcl2* and *Il7r* were similarly more strongly expressed relative to the other clusters in
170 OCA-B- compared to empty vector-transduced cells. These results are consistent with the bulk RNA-
171 seq in that at single-cell resolution we identify memory progenitor clusters with increased *Tcf7* and *Il7r*
172 in the background of global decreases. *Foxo1* was not over-represented in either memory-associated
173 empty vector cluster but was enriched in OCA-B cluster 3. Feature plots showing representative genes
174 in the two sets of clusters are shown in Fig. 3 C. These findings suggest that OCA-B transduced cells
175 in cluster 3 are qualitatively superior to their empty vector-transduced counterparts at forming
176 memory.
177 Clustering empty vector- and OCA-B-transduced cells together allows the relative proportions
178 of cells with common gene expression features to be determined. Again, specific clusters were
179 enriched for effector cells (Fig. 3 D, clusters 0, 1, 4, 6), proliferating effector cells (5) and effector cells
180 with memory progenitor potential (2 and 3). Feature plots for key genes are shown in Fig. 3 E. Cluster
181 2, which was enriched for genes associated with both effector and memory activity (e.g. *Ifng*, *Zeb2*)
182 harbored >3-fold more cells in the OCA-B expressing condition compared to controls (33% vs. 10%),
183 however cluster 3 was also associated with memory (Fig. 3 E) but contained fewer than half as many
184 cells. Although there were fewer cells in cluster 3, analysis of gene expression levels (Fig. 3 F) showed
185 that *Il7r*, *Zeb2* and *Gadd45b* gene expression were elevated in OCA-B-transduced cells. *Foxo1*, *Tcf7*
186 and *Tox* by contrast were expressed similarly. Together these findings identify changes in gene
187 expression and effector T cell populations that predict increased memory potential.
188
189 **OCA-B knock-in reporter mice label CD4$^+$ memory T cell populations**
190 To monitor OCA-B expression in viable cells, we knocked 3 mCherry reporter cassettes preceded by
191 P2A elements into the mouse *Pou2af1* (*Ocab*) locus. The resulting reporter allele contained the
192 mCherry cassettes inserted immediately before the stop codon and the 3' UTR (Fig. S2 A). A
193 successful hemizygous knock-in founder and a homozygote generated by intercrossing the progeny
194 were confirmed by PCR (Fig. S2 B). Hemizygous and homozygous reporter mnice retained normal
195 OCA-B protein expression (Fig. S2 C). We used flow cytometry to identify peripheral blood mCherry-
196 expressing cells from hemizygous and homozygous reporter mice and wild-type controls. OCA-B was
197 readily detectable in B cells (Fig. S2 D, E). Peripheral T cell expression was weaker, forming a
198 shoulder in hemizygous reporters, but a discrete peak in homozygotes (Fig. S2 D, E). We therefore
199 used heterozygous mice to characterize B cell populations, and homozygous mice to study T cells.
200 Robust mCherry expression could be detected in the bone marrow, peritoneal cavity, spleen
201 and lymph nodes of specific pathogen-free hemizygous reporter mice. Total thymocytes by contrast

202 expressed little OCA-B (Fig. S2 F). We used IgM and B220 to discriminate developing, immature and
203 recirculating bone marrow B cells. OCA-B expression was readily detected in developing, immature
204 and recirculating B cell populations compared to wild-type controls (Fig. S2 G). Expression was nearly
205 uniform in the different populations, except for a small population of immature B cells that lacked
206 OCA-B expression. Peritoneal B-1 and B-2 B cells were also homogeneous, with stronger expression
207 in B-2 relative to B-1 cells (Fig. S6 H). Splenic B cells can be partitioned into transitional and mature
208 populations based on CD93 (AA4.1) staining. T1/2/3 subsets stratified by CD23 and IgM uniformly
209 expressed OCA-B (Fig. S6 I). CD21 and CD23 expression divides mature splenic B cells into marginal
210 zone (MZ), follicular and non-follicular populations, and all three populations expressed OCA-B
211 strongly (Fig. S6 J). Expression was largely uniform, but there was a significant population of newly
212 formed $CD21^{lo}CD23^{lo}$ B cells expressing no OCA-B. The nature and significance of these cells is
213 unknown. These results document strong reporter activity in B cell populations, with the highest level
214 of activity in MZ and B-1 B cells. MZ B cells are largely absent in OCA-B knockout mice (Samardzic
215 et al., 2002). These results indicate that the OCA-B reporter robustly labels B cells.
216 Gating out B cells, approximately 5% of thymocytes from unchallenged, specific pathogen-free
217 homozygous reporter mice expressed OCA-B (Fig. S2 K). mCherry expression could be identified in
218 CD4/CD8 double-negative (DN), DP and SP compartments, with the highest amounts in DN and CD8
219 SP cells (Fig. S2 L). In the spleen, the relative abundance of $CD4^+$ and $CD8^+$ T cells was unaltered by
220 the homozygous reporter allele (Fig. 4 A). Splenic $CD4^+$ T cells express mCherry at ~50-fold lower
221 levels compared to B cells and with a wider range of expression (Fig. 4 B). Peripheral blood T cell
222 mCherry levels varied over a similar range (not shown).
223 We used CD62L and CD44 to stratify resting splenic $CD4^+$ and $CD8^+$ cells into naïve,
224 activated/effector and central memory compartments. Reporter activity could be detected in
225 approximately 7% of naïve ($CD62L^{hi}CD44^{lo}$) cells (Fig. 4 C). The nature of these cells (e.g., Tregs,
226 Tscm, recent thymic emigrants) is unknown. Progressively larger fractions of early activated
227 ($CD62L^{lo}CD44^{lo}$), late activated ($CD62L^{lo}CD44^{hi}$) and T_{CM} ($CD62L^{hi}CD44^{hi}$) cells expressed mCherry
228 (Fig. 4 C). Naïve $CD8^+$ T cells showed comparatively higher expression levels, but decreased
229 expression in the activated state and similar expression in T_{CM} cells (Fig. 4 D). Therefore, within the
230 $CD4^+$ T cell compartment, increased OCA-B expression as measured by mCherry fluorescence
231 progressively labels greater fractions of naïve, activated and central memory $CD4^+$ cells.
232
233 **Elevated OCA-B expression prospectively enriches memory precursor $CD4^+$ T cells**

234 To assess OCA-B responses during infection, memory formation and rechallenge, we infected reporter
235 mice with LCMV and used MHC tetramers to identify splenic T cells recognizing immunodominant
236 LCMV epitopes. Prior to infection, >90% of cells were naïve phenotype, with 13.7% of these
237 mCherry^{+}. ~50% of activated CD44^{hi} cells expressed mCherry (Fig. S3 A, D0). Similarly, 50% of 8
238 dpi effector cells expressed mCherry regardless of tetramer status (Fig. S3 B, D8). After LCMV
239 clearance, memory timepoint mice showed higher percentages of mCherry (D43, 61.6%), though with
240 lower expression per cell. Rechallenge with Lm-gp61 to generate CD4^{+} T cell antigen-specific recall
241 responses reduced mCherry positivity compared to resting memory, and high-affinity tetramer^{+} cells
242 declining from >60% to <10% mCherry (Fig. S3 A, D42+7). In contrast, a higher percentage of CD8^{+}
243 reporter T cells expressed mCherry prior to infection. Higher percentages of tetramer^{+} mCherry^{+} were
244 also present at 5 dpi, but by 8 dpi (peak T cell response) mCherry was reduced (Fig. S3 B). Antigen
245 specific memory CD8^{+} T cells also showed reduced mCherry levels relative to CD4^{+} (Fig. S3 B). We
246 did not collect data on CD8^{+} rechallenge because Lm-gp61 does not express the CD8-dominant
247 epitope recognized by H2-D^{b} LCMV tetramers.

248 To determine if OCA-B expression in responding CD4^{+} T cells is associated with increased
249 memory potential, we crossed the reporter allele to a SMARTA TCR transgenic background to fix the
250 TCR specificity and to the Ly5.1 congenic marker to track engrafted cells. We transferred cells into
251 recipients, infected with LCMV, isolated mCherry^{hi} and mCherry^{lo} cells at 8 dpi, transferred large
252 numbers of cells (8×10^{5}) into naïve secondary recipient mice, and isolated splenic CD4^{+} T cells to
253 assess contraction (Fig. 5 A). More cells were recovered from mice engrafted with mCherry^{hi} cells,
254 indicating that these cells contracted less than mCherry^{lo} controls (Fig. 5 B, C). Interestingly the degree
255 of mCherry fluorescence in the cells that did survive was the same in both groups, though with
256 considerably more variance associated with mCherry^{lo} (Fig. 5 D) These findings suggest that effector
257 CD4^{+} cells expressing higher OCA-B undergo less cell death.

258 To test the ability of the cells expressing OCA-B to mount antigen recall responses, we
259 similarly transferred congenically marked SMARTA cells into recipient mice and infected with
260 LCMV, but isolated mCherry^{hi} and mCherry^{lo} cells at 43 dpi. 4×10^{4} of memory SMARTA cells were
261 transferred into naïve hosts, which were challenged with LCMV and analyzed at 7 dpi (Fig. 5 E).
262 mCherry^{hi} SMARTA cells mounted better recall responses compared to mCherry^{lo} (Fig. 5 F, G) though
263 again with little difference in mCherry fluorescence (Fig. 5 H). This result indicates a plasticity in
264 OCA-B expression whereby expression normalizes following antigen re-encounter.

265 In mice, OCA-B expression can be detected, varying over a 10-fold range, in responding cells
266 as early as one day after infection with lymphocytic choriomeningitis virus (LCMV) (Shakya et al.,
267 2015). Memory progenitor cells characterized by low CD25 expression can be identified as early as
268 early as 3 dpi (Snook et al., 2018). We transferred SMARTA homozygous OCA-B mCherry reporter T
269 cells into congenic recipients, infected with LCMV, and collected spleens at 3 dpi to study mCherry
270 and CD25 levels (Fig. 5I). A large fraction of responding $CD25^{lo}$ SMARTA cells expressed mCherry
271 (Fig. 5J). SMARTA cells from the same mouse expressing low levels of CD25 also expressed high
272 levels of TCF1, as expected (Snook et al., 2018). mCherry and TCF1 were not compared as cell
273 fixation quenches mCherry, however we were able to directly compare CD25 and OCA-B. $CD25^{hi}$
274 cells expressed a range of OCA-B, while $CD25^{lo}$ cells were highly enriched for $mCherry^{hi}$ cells (Fig.
275 5K, L). These findings show that high OCA-B expression can be used as a method to prospectively
276 mark live $CD4^{+}$ memory precursor effector T cells with augmented capacity to form central memory.
277 Identifying transcriptional regulators that define the memory precursor effector $CD4^{+}$ T cells will
278 promote advances in understanding the formation of CD4 T cell memory. Cumulatively, this study
279 indicates that OCA-B expression within $CD4^{+}$ T cells is both necessary for, and sufficient to promote,
280 the emergence of T_{CM}.

281 **Materials and methods**

282 **Mice**

283 All mice used in this study were on the C57BL6/J strain background. All mouse experiments were
284 approved by the University of Utah Institutional Animal Care and Use Committee (protocol
285 00001553). *Pou2af1* (*Ocab*) conditional (floxed) mice were described previously (Kim et al., 2021).
286 *Pou2af1*-3×mCherry reporter knock-in mice were generated on a C57BL/6N background
287 (Biocytogen), but were backcrossed >5 times to C57BL/6J prior to generation of data herein.

288

289 **LCMV and *Listeria* infection**

290 LCMV Armstrong 53b ($LCMV^{Arm}$) (Ahmed et al., 1984) was grown in BHK cells and titered using
291 Vero cells (Oxenius et al., 1998). For primary infection, 8-to 12-week-old $Ocab^{fl/fl}$ or $Ocab^{fl/fl}$;CD4-Cre
292 mice were inoculated i.p. with 2×10^5 plaque-forming units (PFU) of LCMV intraperitoneally.
293 For heterologous rechallenge with *Listeria monocytogenes* expressing LCMV glycoprotein 61-80 (Lm-
294 gp61) (Shen et al., 1995), bacteria were grown in log phase in BHI media, and concentrations were
295 calculated using OD at 600 nm (OD of $1=1\times10^9$ CFU/mL). Mice were rechallenged intravenously with
296 2×10^5 colony forming units (CFU) of Lm-gp61 the indicated number of days after primary infection as
297 published (Kim et al., 2012).

298

299 **Bone marrow radiation chimeras**

300 Radiation chimeras were generated as published (Mitchell et al., 2010). Briefly, male Ly5.1 C57BL/6J
301 mice were used as recipients. Mice received a split dose of 900 Rad (2×450 RAD, spaced 1 hr apart),
302 and were engrafted one day later with 1 million mixed donor bone marrow cells. Competitor bone
303 marrow cells from Ly5.2/Thy1.1 but otherwise wild-type mice, and experimental cells from
304 Ly5.2/Thy1.2 $Ocab^{fl/fl}$ or littermate $Ocab^{fl/fl}$;CD4-Cre mice, were isolated from femurs and tibias of
305 donor mice. After red blood cell lysis, $CD3^+$ cells were depleted using biotinylated anti-CD3
306 antibodies (eBioScience) and anti-biotin magnetic MicroBeads (Miltentyi Biotech) according to the
307 manufacturer's instructions. CD3-depeleted bone marrow cells were mixed 1:1 and injected retro-
308 orbitally. The chimeras were rested for 8 weeks to allow engraftment, after which mice were infected
309 as above. Virus-reactive cells were identified by $LCMVgp_{66–77}$:I-Ab tetramer staining.

310

311 **pMSCV-IRES-GFP-OCA-B vector generation**

312 Wild-type *Ocab* cDNA was amplified from the plasmid pcDNA3.1-OCA-B (Luo and Roeder, 1995) (a
313 gift from Robert Roeder, Rockefeller University) by PCR and cloned into the pMSCV-IRES-GFP
314 (pMIGR1) retroviral vector (a gift from Ryan O'Connell, University of Utah). Primers used for
315 amplification were mOcab-F-XhoI, 5'CTCGAGCTGTCTGCTTCAAAGAGAAAAGGCAAC;
316 mOcab-R-*Eco*RI, 5' GAATTCCTAAAAGCCCTCCACGGAGAGGGT. The PCR product was gel
317 purified, digested with *Eco*RI and *Xho*I, and inserted into a similarly digested pMIGR1 backbone using
318 T4 DNA ligase to generate pMIG-OCA-B. All constructs were validated by resequencing.
319
320 **CD4$^+$ T cell isolation and stimulation**
321 Naïve splenic CD4$^+$ T cells were isolated and simulated as described previously (Shakya et al., 2011).
322 Briefly, spleens were dissociated by grinding and passing through a 70 μm nylon strainer. Red blood
323 cells were lysed by ACK lysis buffer (150 mM NH_4Cl, 10 mM $KHCO_3$, 0.1 mM EDTA). Cells were
324 isolated from mice using a naïve CD4$^+$ T cell isolation kit (Miltenyi), and stimulated in culture using
325 10 μg/mL plate-bound anti-CD3ϵ and 2 μg/mL anti-CD28 antibodies (eBioscience).
326
327 **Ectopic OCA-B expression in CD4$^+$ T cells**
328 T cells from Ly5.1 SMARTA and Thy1.1 SMARTA mice were purified using a CD4$^+$ T cell isolation
329 kit (Miltenyi). Cells were placed into RPMI 1640 medium supplemented with 10% fetal bovine serum,
330 50 U/mL penicillin, 50 μg/mL streptomycin, 2 mM L-glutamine, 1 mM sodium pyruvate, 1× MEM
331 nonessential amino acids, 55 μM 2-mercaptoethanol, and 20 IU/mL recombinant human IL-2. All
332 components were from ThermoFisher with the exception of IL-2, which was supplied by R&D
333 Systems. Cells were simultaneously transduced with pMIGR retroviruses packaged in 239T cells, with
334 or without expressed mouse OCA-B cDNA, using spin infection. For spin infection, cells were
335 centrifuged with 293T retroviral supernatant at 1000×*g* for 2 hr at 37°C in the presence of 4 μg/mL
336 polybrene (Sigma). On the following day, transduced GFP$^+$ cells were isolated by fluorescent-activated
337 cell sorting. 2×10^4 pMIGR1- and pMIGR1-OCA-B-transduced cells were combined and co-transferred
338 into wild-type (Ly5.2/Thy1.2) C57BL6/J mice. Chimeric mice were infected with LCMV and re-
339 challenged with Lm-gp61 as described above.
340
341 **Flow cytometry**
342 Spleens were dissociated and passed through a 70 μm nylon strainer. Red blood cells were lysed by
343 ACK lysis buffer (150 mM NH_4Cl, 10 mM $KHCO_3$, 0.1 mM EDTA). For intracellular staining, cell

344 suspensions in RPMI supplemented with 10% fetal bovine serum were re-stimulated for 4 hr with 1
345 μM LCMV $GP_{61–80}$ or 0.1 μM GP_{33-41} peptide along with Brefeldin A (GolgiPlug Becton-Dickinson, 1
346 μl/mL) as published (Murali-Krishna et al., 1998; Williams et al., 2008). Cells were subsequently fixed
347 by cell fixation/permeabilization solution (Cytofix/Cytoperm, Becton-Dickinson) according to the
348 manufacturer's protocol. For tetramer staining, APC-conjugated $gp_{66–77}$:I-A^b and gp_{33-41}:H-$2D^b$
349 tetramers were provided by the NIH Tetramer Core Facility (Emory Vaccine Center). Cell suspensions
350 were incubated at 37°C for 3 hr in RPMI with the tetramer followed by cell-surface staining. Tetramer
351 fluorescence was normalized with isotype tetramer (hCLIP:I-A^b) staining. Antibodies used for flow
352 cytometry are presented in the Key Resources Table.
353
354 **Bulk RNAseq**
355 $CD4^+$ T cells were purified from female Ly5.1 SMARTA and Ly5.1/5.2 SMARTA mice, and
356 separately transduced with pMIG-OCA-B or empty vector (EV), respectively. On the following day,
357 transduced GFP^+ cells were sorted, 20,000 of each combined 1:1, and injected intravenously into 24
358 male C57BL/6J male recipients. 24h later, each recipient mouse was injected intraperitoneally with
359 $2x10^5$ pfu LCMV. After eight days, the 24 mice were divided into six groups of four mice by
360 combining four spleens together. $CD4^+$ T cells were purified using a Miltenyi CD4 T cell isolation kit.
361 Cells then were stained with PerCP-Cy5.5 Ly5.1 and AF700 Ly5.2 antibodies. $GFP^+Ly5.1^+Ly5.2^+$
362 (EV) and $GFP^+Ly5.1^+$ (OCA-B-expressing) cells were sorted by fluorescence-activated cell sorting
363 (FACS) and used for RNA purification (RNeasy Mini Kit, QIAGEN). RNA concentrations were
364 determined using a Quant-iT RNA assay kit and a Qubit fluorometer (ThermoFisher). Because limited
365 RNA from EV-transduced cells was obtained, the six EV samples were combined into three samples.
366 Five OCA-B-transduced samples (each comprising four mice) were submitted for RNAseq analysis.
367 These showed a high degree of concordance (not shown). Total RNA samples (200-500 ng) were
368 hybridized with Ribo-Zero Plus (Illumina) to deplete cytoplasmic and mitochondrial and ribosomal
369 RNA from samples. RNA sequencing libraries were prepared as described using the Stranded Total
370 RNA Prep, Ligation with Ribo-Zero Plus kit (Illumina) and IDT for Illumina RNA UD Indexes Set A,
371 Ligation (Illumina). Purified libraries were qualified on an Agilent Technologies 2200 TapeStation
372 using a D1000 ScreenTape assay. The molarity of adapter-modified molecules was defined by qPCR
373 using the Kapa Biosystems Kapa Library Quant Kit. Individual libraries were normalized to 0.65 nM
374 in preparation for Illumina sequence analysis. Sequencing libraries were chemically denatured and
375 applied to an Illumina NovaSeq flow cell using the NovaSeq XP workflow (20043131). Following

376 transfer of the flow cell to an Illumina NovaSeq 6000 instrument, a 150 x 150 cycle paired-end
377 sequence run was performed using a NovaSeq 6000 S4 reagent Kit v1.5 (Illlumina).
378
379 **Bulk RNA-seq analysis**
380 Bulk RNA-seq analysis was performed as previously described (Perovanovic et al.). Briefly, Reads
381 were aligned to *Mm10* using STAR (v2.7.3a) and checked for quality using multiqc (v1.10). Between
382 12 and 14 million pair-end reads were generated for each sample, with >98% of aligned reads mapping
383 to the correct strand and >93% of the reads uniquely aligned to the gene. Differentially expressed
384 genes were identified using DESeq2 version 1.24.0 (Love et al., 2014) with a 5% FDR cutoff. Features
385 with zero counts and 5 or fewer reads in every sample were removed from the analysis. Genes
386 increased by 1.4-fold or more or decreased by 2-fold or more, and with adjusted $p<0.05$ were selected
387 as differentially expressed ($0.5 < \log2FC < -1$; padj ≤ 0.05). Figures were generated in R version 4.0.0
388 using functions from ggplots libraries and pheatmap.
389
390 **Single-cell RNA-seq**
391 To profile gene expression at the single-cell level, splenic $GFP^{+}Ly5.1^{+}Ly5.2^{+}$ (EV-transduced) and
392 $GFP^{+}Ly5.1^{+}$ (OCA-B-transduced) SMARTA cells from four pooled mice per condition were isolated,
393 resuspended in PBS with 0.04% bovine serum albumin (ThermoFisher), and filtered through 40 μm
394 strainers. Viability and cell count were assessed using a Countess II (ThermoFisher). Equilibrium to
395 targeted cell recovery of 6,000 cells along with Gel Beads and reverse transcription reagents were
396 loaded to Chromium Single Cell A to form Gel-bead-in Emulsions (GEMs). Within individual GEMs,
397 cDNA generated from captured and barcoded mRNA was synthesized by reverse transcription at 53°C
398 for 45 min. Samples were then heated to 85°C for 5 min. Single cell transcriptomes were assessed
399 using a 10X Genomics Chromium Single Cell Gene Expression instrument. Individual cells were
400 tagged with 16 bp barcodes, and specific transcripts with 10 bp Unique Molecular Identifiers (UMIs)
401 according to manufacturer instructions.
402
403 **Single-cell RNA-seq analysis**
404 Single cell transcriptome data were analyzed and clustered as described previously (Perovanovic et
405 al.). Sequences from the Chromium platform were de-multiplexed and aligned using CellRanger ver.
406 3.1.0 (10X Genomics) with default parameters mm10-3.0.0. Clustering, filtering, variable gene
407 selection and dimensionality reduction were performed using Seurat ver.4.0.4 (Stuart et al., 2019)

408 according to the following workflow: 1, Cells with <200 detected genes were excluded further
409 analysis. 2, Cells with <5% UMIs mapping to mitochondrial genes and *Cd44* expression >0 were
410 retained for downstream analysis, , as SMARTA cells are uniformly responding to LCMV
411 glycoprotein antigen at this time. 3, The UMI counts per ten thousand were log-normalized for each
412 cell using the natural logarithm. 4, Variable genes (2000 features) were selected using the
413 FindVariableFeatures function. 5, Common anchors between the conditions were identified using
414 FindIntegrationAnchors function that were further used to integrate these sets. 6, Gene expression
415 levels in the integrated set were scaled along each gene and linear dimensional reduction was
416 performed. The number of principal components was decided through the assessment of statistical
417 plots (JackStrawPlot and ElbowPlot). 7, Cells were clustered using a shared nearest neighbor (SNN)
418 modularity optimization-based clustering algorithm and visualized using two-dimensional uniform
419 manifold approximation and projection (UMAP). 8, One cluster in each condition marked
420 predominantly by mitochondrial genes (indicative of dying cells) was excluded from the analysis. This
421 resulted in 12,886 empty vector-transduced cells with 45,748 mean reads per cell, and 2,595 median
422 genes per cell. The total number of reads was 589,513,069, with 59.6% mapping to exonic regions.
423 Similarly, there were 11,709 OCA-B-transduced cells with 68,931 mean reads per cell, and 2,668
424 median genes per cell. Total number of reads was 807,111,486, with 57.4% mapping to exonic regions.
425 Clusters were identified using manual interrogation of gene expression enrichment for each population
426 (Table S3), the ImmGene cluster identity predictor (Table S4, S5), and PanglaoDB annotation terms.
427

428 **Memory progenitor isolation, normalization and transfer**

429 To assess contraction of the effector cells with different OCA-B levels, splenic $CD4^+$ T cells were
430 purified from 8 week-old female Ly5.1/5.2 homozygous knock-in reporter, SMARTA TCR transgenic
431 mice. 2×10^4 SMARTA cells were intravenously injected into 15 male Ly5.2/5.2 C57BL/6J recipients,
432 which were infected intraperitoneally 1 day later with 2×10^5 plaque-forming units of LCMV in 250 μL
433 phosphate-buffered saline. After 8 days, responding $Ly5.1^+5.2^+$ SMARTA T cells were sorted into
434 $mCherry^{hi}$ and $mCherry^{lo}$ populations. Cells were pooled and 8×10^5 $mCherry^{hi}$ and $mCherry^{lo}$ cells
435 were separately injected intravenously into 7 naïve age-matched 9 week-old male C57BL/6J secondary
436 recipients in the case of $mCherry^{lo}$ and 5 secondary recipients in the case of $mCherry^{hi}$. After 8
437 additional days, mice were sacrificed and splenic $Ly5.1^+5.2^+$ SMARTA cells were counted by flow
438 cytometry. To assess proliferative responses to rechallenge, 15 similar virus-naïve secondary recipients
439 were rested for 43 days post-infection prior to isolation of $mCherry^{hi}$ and $mCherry^{lo}$ populations.

440 1.3×10^4 SMARTA cells were transferred into naïve recipients, which were infected with LCMV one
441 day later. 7 days post-infection, splenic $CD4^+Ly5.1^+5.2^+$ SMARTA cells were evaluated by flow
442 cytometry. Mice with poor infection/response (total splenocyte count $<6\times10^7$) were excluded from the
443 analysis.
444

445 **Quantification and statistical analysis**

446 Excel (Microsoft) and Prism (GraphPad) were used for statistics and graphing. Two-tailed Student T-
447 tests were used to ascribe statistical significance unless otherwise indicated. For all figures, *=*p*-
448 value≤0.05; **=*p*≤0.005; ***=p<0.001. All error bars denote ± standard error of the mean.

449 **Acknowledgements:** We thank M. Chandrasekharan for help with graphics. We thank J. Marvin and
450 the University of Utah Health Sciences Center Flow Cytometry Core facility. We thank O. Allen, B.
451 Dalley and the High-Throughput Genomics Core. MHC tetramers were provided by the NIH Tetramer
452 Core Facility (Atlanta, GA). We thank R. Roeder for the mouse OCA-B cDNA and R. M. O'Connell
453 for the pMIGR1 plasmid.
454
455 **Funding:** This work was supported by NIH grant R01AI100873 to DT.
456
457 **Author's contributions:**
458 Conceptualization: DT
459 Methodology: WS, HK, JP, MAW
460 Investigation: WS, HK, EH, JD, AI
461 Visualization: WS, HK, JP
462 Funding acquisition: DT
463 Project administration: DT
464 Supervision: JSH, MAW, DT
465 Writing – original draft: WS, HK, JP, EH, JD, AI, JSH, MAW, DT
466
467 **Competing interests:** The authors declare that they have no competing interests.
468
469 **Data and materials availability:** All data are available in the main text or the supplementary
470 materials. Materials used in the study are available to any researcher for purposes of reproducing or
471 extending the findings. Bulk and single-cell RNA-seq data have been deposited at the Gene Expression
472 Omnibus GEO) website (https://www.ncbi.nlm.nih.gov/geo/, GSE214310).

473 **Figures legends**

474 Figure 1. **Ectopic OCA-B expression enhances CD4$^+$ T cell memory recall responses in vivo.**
475 **(A)** Experimental schematic for OCA-B transduction and T cell mixed adoptive transfer. Ly5.1$^+$
476 SMARTA cells were transduced with pMSCV-IRES-GFP (pMIG) empty vector (EV) and Thy1.1$^+$
477 SMARTA cells were transduced with pMIG expressing mouse OCA-B (pMIG-OCA-B). The donors
478 were age- and sex-matched littermates. Following transduction, the two populations of SMARTA cells
479 were combined 1:1, co-transferred into Ly5.2$^+$/Thy1.2$^+$ C57BL6/J recipient mice, and infected with
480 LCMV. Recipients were rechallenged with Lm-gp61 on either day 52 or 110 post-LCMV infection,
481 and in each case analyzed after 7 days. **(B)** Lysates from 3T3 cells transduced with either empty pMIG
482 empty vector (EV) or pMIG-OCA-B were immunoblotted using antibodies against OCA-B. α-tubulin
483 is shown as an internal loading standard. **(C)** Flow cytometric analysis of Ly5.1$^+$ pMIG empty vector-
484 transduced (EV) and Thy1.1$^+$ pMIG-OCA-B-transduced (OCA-B) SMARTA cells in the spleen and
485 blood of a representative recipient mouse at peak effector response (D8), peak memory recall response
486 (52+7) and long-term memory recall (D110+7). Cells were first gated based on CD44, CD4 and GFP
487 positivity. **(D)** Mean relative percentages of splenic and blood total EV- or pMIG-OCA-B-transduced
488 (GFP$^+$) SMARTA cells were plotted at D8, D52+7 and 110+7. Each datapoint represents an individual
489 mouse harboring both EV- or pMIG-OCA-B-transduced cells. 5, 7 and 10 mice were sacrificed at each
490 timepoint to obtain measurements from spleen. All mice were bled at D8, and remaining mice were
491 bled at subsequent timepoints. **(E)** Mean ratios of pMIG-OCA-B-transduced relative to empty vector-
492 transduced SMARTA cells (OCA-B/EV) are plotted. Splenic (top) and peripheral blood (bottom)
493 SMARTA T cells are shown at day 8 post-infection, or 7 days post-rechallenge with Lm-gp61 (52+7
494 or 110+7). **(F)** Flow cytometry showing relative percentages of splenic GFP$^+$CD44^{hi} EV-transduced
495 (blue) or pMIG-OCAB-transduced (red) SMARTA cells expressing ICOS, PD-1, Ly6C or CD62L at
496 day 8 post-infection. Representative data showing the two populations of cells within a single mouse
497 are shown at day 8 post-infection. **(G)** Percent expression for ICOS, PD-1, CD62L and Ly6C was
498 quantified from four mice using splenic EV- and pMIG-OCAB-transduced GFP$^+$CD44^{hi} SMARTA
499 cells at 8 days post-infection. Four replicates were performed. For CD26L, the four datapoints are
500 superimposed, and for Ly6C two of the datapoints are superimposed. Individual mice are connected by
501 lines.

502

503 Figure 2. **Gene expression changes associated with ectopic OCA-B expression in SMARTA**
504 **transgenic primary effector T cells. (A)** Heatmap showing top up- and down-regulated genes. Genes

505 with log2 fold-change >0.5 or <-1.0, and padj ≤ 0.05 are shown. Example genes are shown at right.
506 Control and OCA-B-transduced cells were purified from the same mice using magnetic isolation and
507 FACS. **(B)** Example genome tracks showing two up-regulated genes, *Socs2* and *Gadd45b*. *Pou2af1*
508 (*Ocab*) is shown as a positive control. **(C)** Top Epigenomic roadmap and Molecular function GO terms
509 for the set of OCA-B up- and down-regulated genes. **(D)** Top ChIP-X Enrichment Analysis (ChEA
510 2016) factors potentially regulating the same set of genes up- and down-regulated by OCA-B ectopic
511 expression.
512
513 Figure 3. **Single-cell RNA-seq analysis of SMARTA cells transduced with OCA-B or empty**
514 **vector. (A)** UMAP projections of independently clustered empty vector-transduced (GFP^+) SMARTA
515 cells purified similar to Figs. 2 and 3, and subjected to scRNA-seq. Cluster identities were annotated
516 using a combination of gene expression enrichment (Table S3), cluster identity predictor ImmGen
517 identity scores (Table S4) and PanglaoDB annotation terms. Clusters 1 and 4 were associated with
518 memory formation. Top PanglaoDB annotation terms for cluster 4 are shown below. **(B)** Similar
519 UMAP projection using OCA-B-transduced cells purified from the same mice as in (A). Cluster
520 identities were annotated similarly to (A). Cluster 3 in OCA-B-transduced cells was most strongly
521 associated with memory formation. Top PanglaoDB annotation terms for cluster 3 are shown below.
522 **(C)** Feature plots highlighting expression of representative genes for the two UMAP projections in (A)
523 and (B). **(D)** UMAP projections of the the EV- and OCA-B-transduced single-cell RNA-seq datasets
524 clustered together. For each projection, the percentage of each cluster relative to the total number cells
525 in condition is shown. Cluster identities were annotated using a combination of gene expression
526 enrichment (Table S3), cluster identity predictor ImmGen identity scores (Table S5) and PanglaoDB
527 annotation terms. **(E)** Feature plots highlighting expression of representative genes for the combined
528 projections.
529 **(F)** Violin plots depicting expression of six genes (*Il7r*, *Zeb2*, *Gadd45b*, *Foxo1*, *Tcf7* and *Tox*) across
530 each of the 10 clusters in EV-transduced cells (blue, left) and OCA-B-transduced cells (red, right).
531
532 Figure 4. **mCherry expression in splenic T cell populations in specific pathogen-free homozygous**
533 **OCA-B-3×mCherry mice. (A)** CD4 and CD8 expression are shown for an allelic series of example
534 wild-type (+/+) and homozygous (KI/KI) OCA-B knock-in reporter mice. **(B)** OCA-B homozygous
535 reporter expression in splenic $CD4^+$ T cell populations. **(C)** The same $CD4^+$ cells as in (B) were further
536 stratified by CD62L and CD44 into naïve effector (Teff) and central memory (Tcm) populations.

537 $CD62L^{lo}CD44_{lo}$ cells are likely recently activated cells that have down-regulated CD62L but not yet
538 up-regulated CD44. **(D)** Similar analysis as in (C) except for $CD8^+$ cells.
539
540 Figure 5. **$CD4^+$ T cells expressing high levels of OCA-B reporter activity preferentially form**
541 **central memory cells. (A)** Schematic for assessing contraction of $mCherry^{hi}$ vs. $mCherry^{lo}$ SMARTA
542 T cells following LCMV infection. Congenically marked SMARTA T cells were isolated from donor
543 mice, transferred into naïve secondary recipients and infected with LCMV. At 8 days post-infection,
544 $mCherry^{hi}$ and $mCherry^{lo}$ populations were isolated by FACS. 8×10^5 SMARTA cells were transferred
545 into naïve recipients. After 8 days, splenic $CD4^+Ly5.1^+5.2^+$ SMARTA cells were evaluated by flow
546 cytometry. **(B)** Flow cytometric analysis of SMARTA donor T cells engrafted into naïve mice to
547 monitor rates of decline. Representative mice engrafted with $mCherry^{lo}$ (left) or $mCherry^{hi}$ (right) cells
548 are shown. **(C)** Quantification of averaged donor T cell numbers from mice engrafted with $mCherry^{lo}$
549 or $mCherry^{hi}$ cells. N=7 for the $mCherry^{lo}$ group and N=5 for the $mCherry^{hi}$ group. **(D)** Similar analysis
550 to (C) except quantifying mean mCherry fluorescence intensity. **(E)** Schematic for assessing recall
551 responses of $mCherry^{hi}$ vs. $mCherry^{lo}$ SMARTA T cells following LCMV infection. Congenically
552 marked SMARTA T cells were isolated from donor mice, transferred into naïve secondary recipients
553 and infected with LCMV. However, mice were allowed to clear LCMV and form memory. After 43
554 days, $mCherry^{hi}$ and $mCherry^{lo}$ memory T cell populations were isolated by FACS. 1.3×10^4 SMARTA
555 cells were transferred into naïve recipients, which were infected with LCMV one day later. 7 days
556 post-infection, splenic $CD4^+Ly5.1^+5.2^+$ SMARTA cells were evaluated by flow cytometry. **(F)** Flow
557 cytometric analysis of SMARTA donor T cells 7 days post-rechallenge to monitor recall responses.
558 Representative mice engrafted with $mCherry^{lo}$ (left) or $mCherry^{hi}$ (right) cells are shown. **(G)**
559 Quantification of averaged donor T cell percentages and numbers from mice engrafted with $mCherry^{lo}$
560 or $mCherry^{hi}$ cells. N=7 for the $mCherry^{lo}$ group and N=5 for the $mCherry^{hi}$ group. **(H)** Similar
561 analysis to (G) except quantifying mean mCherry fluorescence intensity. (**I**) Schematic for assessing
562 mCherry levels in SMARTA T at early timepoints following LCMV infection. 2×10^5 congenically
563 marked ($CD45.1^+$) SMARTA T cells were isolated from donor mice and transferred into naïve
564 secondary recipients. One day later mice were intraperitoneally infected with 2×10^5 PFU LCMV.
565 Splenic T cells were collected at 3 dpi. (**J**) Gated unfixed splenic $CD4^+$ T cells were assessed for the
566 SMARTA congenic marker Ly5.1 and mCherry (left), while fixed $Ly5.1^+$ (SMARTA) cells from the
567 same mice were used to assess CD25 and TCF1 (right). (**K**) CD25 and mCherry expression were
568 assessed from a representative animal. Left: distribution of SMARTA cell CD25 and mCherry

569 expression in SMARTA mice. Right: CD25 levels of gated mCherry^{hi} and mCherry^{lo} SMARTA cells
570 displayed as a concatenated histogram. (**L**) Quantification of averaged mCherry MFI in CD25^{hi} and
571 CD25^{lo} cells (left), and frequencies (center) and numbers (right) of CD25^{lo} cells in mCherry^{lo} or
572 mCherry^{hi} cells SMARTA T cells. N=6 independent recipient mice.
573
574 **Supplementary Materials**
575 Figure S1. **OCA-B in T cells is required for robust polyclonal memory CD4+ T cell formation and**
576 **cytokine expression following LCMV infection. (A)** *Ocab$^{fl/fl}$*;CD4-Cre and control *Ocab$^{fl/fl}$* mice
577 were infected with LCMV and rechallenged with Lm-gp61 40 days after LCMV infection. Splenic I-
578 A^b/gp$_{66–77}$ tetramer-positive, CD4$^+$CD44$^+$ T cells were analyzed by flow cytometry 8 days after
579 primary infection and 7 days after heterologous rechallenge. n=5 for each group. n.s.=not significant.
580 **(B)** Splenocytes from LCMV-infected *Ocab$^{fl/fl}$*;CD4-Cre or control *Ocab$^{fl/fl}$* mice were restimulated in
581 vitro with gp$_{61-80}$ peptide for 4 hours, and IFNγ and IL-2 expression in CD4$^+$ T cells examined by flow
582 cytometry. Cells were gated based on I-A^b/gp$_{66–77}$ tetramer, CD4 and CD44 positivity. Data from
583 representative mice are shown. **(C)** Mean T cell frequencies of CD4$^+$CD44$^+$IFNγ$^+$IL-2$^-$ T cells are
584 shown. n=5 for each group. **(D)** Surface marker expression in polyclonal OCA-B T cell-deficient and
585 control splenic CD4$^+$ effector T cells at 8 days post-infection or 7 days post-rechallenge. Example flow
586 cytometry panels of ICOS, Ly6C, CD62L. PD-1 was additionally performed for memory recall
587 responses. Cells were gated for I-A^b-LCMV$^{gp66-77}$ positivity. **(E)** Flow cytometry plot showing
588 Thy1.1$^+$Ly5.2$^+$ but otherwise genetically wild-type (WT) donor bone marrow cells engrafted 50:50
589 with Ly5.2$^+$ control cells lacking the Cre driver (*fl/fl*) or experimental T cell-conditional *Ocab$^{fl/fl}$*;CD4-
590 Cre donor cells (*fl/fl*;Cre). Recipient hosts were Ly5.1$^+$. Splenic effector cells were recovered at
591 primary response (D8) or seven days post-rechallenge (D42+7). Cells were gated based on I-A^b/gp$_{66–77}$
592 tetramer positivity. Example mice are shown. **(F)** Mean wild-type competitor to control of OCA-B
593 deficient T cell ratios are shown. n=3 for each group.
594
595 Figure S2. **OCA-B-3×mCherry knock-in reporter mouse characterization in B and developing T**
596 **cell populations. (A)** Mouse *Pou2af1* locus, targeting vector and the targeted *Pou2af1* locus. **(B)** PCR
597 genotyping OCA-B-3×mCherry reporter mice. PCR yields a 494 bp product for the wild-type *Pou2af1*
598 allele and a 373 bp product for the targeted *Pou2af1* allele. +=wild-type allele. KI=knock-in allele. **(C)**
599 OCA-B immunoblot using splenocytes from wild-type (+/+) and heterozygous (+/KI) or homozygous
600 knock-in OCA-B-3×mCherry knock-in mice. β-actin was used as a loading control. **(D)** Flow

601 cytometry showing mCherry expression in peripheral blood cells of wild-type mice (+/+), or either
602 heterozygous (+/KI) or homozygous (KI/KI) OCAB-3×mCherry knock-in reporter mice. **(E)** Similar
603 flow cytometry plots as in (D) except gated on the indicated populations. **(F)** mCherry (OCA-B)
604 expression in a 4.5 week-old heterozygous female OCA-B-3×mCherry reporter mouse. Cells were
605 harvested from bone marrow (BM), peritoneal cavity (PC), spleen (SP), lymph node (LN) or thymus.
606 After removal of red blood cells, mCherry expression was measured in total cell populations. **(G)**
607 Wild-type (+/+) and heterozygous knock-in (+/KI) bone marrow cells were further stratified into B1
608 and B2 populations based on B220 and IgM expression Top plots show relative proportions of B1
609 ($IgM^{hi}B220^{lo}$) B2 ($IgM^{lo}B220^{hi}$) cells in wild-type and two example heterozygous reporter mice.
610 Bottom plots show mCherry expression in gated populations. **(H)** Analysis of peritoneal cavity B cell
611 populations from +/+ and +/KI reporter mice. Cells were stratified into pro/pre, immature and
612 recirculating B cell compartments based on B220 and IgM expression. Top plots show relative
613 proportions of the cells in mice of the indicated genotypes. Bottom plots show mCherry levels in the
614 gated populations. **(I)** Splenic transitional B cells were stratified using CD93 (AA4.1), CD23 and IgM
615 antibodies. One wild-type and two example heterozygous reporter mice are shown. **(J)** Similar analysis
616 to (I) except using CD21 and CD23 antibodies to visualize follicular and MZ B cell populations. **(K)**
617 mCherry expression in total B220-negative thymocytes from wild-type (+/+) or homozygous knock-in
618 reporter mice was analyzed by flow cytometry. Specific pathogen-free mice were used. **(L)**
619 Thymocytes were stained with CD4 and CD8 antibodies to visualize double-negative, double-positive
620 and single-positive T cell developmental stages in homozygous knock-in reporter mice. Right:
621 mCherry expression in developing reporter T cells was subdivided by quadrant.
622
623 Fig. S3. **OCA-B expression in antigen-responsive T cells following LCMV infection. (A)** Flow
624 cytometry images are shown of homozygous OCA-B-3×mCherry knock-in reporter mice at different
625 timepoints following LCMV infection (D0-43) and following rechallenge with Lm-gp61. Mice were
626 challenged on different days and spleens were harvested and processed on the same day. Top panels:
627 percentages of cells expressing CD44 and class II LCMV tetramer (I-A^b $LCMV^{gp66-77}$) are shown.
628 Bottom panels: for the same timepoints cells gated from each quadrant in the top panels are plotted.
629 Each flow panel is representative of biological duplicate mice sacrificed at each timepoint. **(B)** Cells
630 from the same mice as above were gated for CD8 expression and stained with class I LCMV tetramers
631 (H2-D^b $LCMV^{gp33-41}$). Analysis of recall response timepoints was not possible for antigen-specific

632 CD8 cells because mice were rechallenged with Lm-gp61, which lacks CD8 immunodominant
633 epitopes.
634
635 Table S1. **Differentially expressed bulk RNAseq genes comparing GFP$^+$ SMARTA T cells**
636 **expressing empty vector or OCA-B at day 8 post-LCMV infection (cutoffs: -1>log2FC>0.5,**
637 ***p*<0.05)**
638
639 Table S2. **Gene Ontology analysis using differentially expressed bulk RNA-seq transcripts**
640 **comparing GFP$^+$ SMARTA T cells transduced with empty vector or OCA-B at day 8 post-**
641 **LCMV infection (cutoffs: -1>log2FC>0.5, *p*<0.05)**
642
643 Table S3. **Single-cell RNA-seq gene enrichments by cluster in GFP$^+$ SMARTA T cells transduced**
644 **with empty vector or OCA-B at day 8 post-LCMV infection.**
645
646 Table S4. **Top 5 single-cell RNA-seq ImmGen identity scores per cluster using GFP$^+$ SMARTA T**
647 **cells transduced with empty vector or OCA-B at day 8 post-LCMV infection.**
648
649 Table S5. **Integrated gene enrichment analysis of single-cell RNA-seq gene enrichments by**
650 **cluster in GFP$^+$ SMARTA T cells transduced with empty vector or OCA-B at day 8 post-LCMV**
651 **infection.**

652 **References and Notes**

653 Ahmed, R., A. Salmi, L.D. Butler, J.M. Chiller, and M.B. Oldstone. 1984. Selection of genetic variants
654 of lymphocytic choriomeningitis virus in spleens of persistently infected mice. Role in
655 suppression of cytotoxic T lymphocyte response and viral persistence. *J Exp Med* 160:521-540.
656 Ban, M., D. Booth, R. Heard, G. Stewart, A. Goris, K. Vandenbroeck, B. Dubois, M. Laaksonen, J.
657 Ilonen, M. Alizadeh, G. Edan, M.C. Babron, D. Brassat, M. Clanet, I. Cournu-Rebeix, B.
658 Fontaine, G. Semana, R. Goedde, J. Epplen, A. Weber, C. Infante-Duarte, F. Zipp, C. Rajda, K.
659 Bencsik, L. Vecsei, S. Heggarty, C. Graham, S. Hawkins, M. Liguori, P. Momigliano-
660 Richiardi, D. Caputo, L.M. Grimaldi, M. Leone, L. Massacesi, C. Milanese, M. Salvetti, G.
661 Savettieri, M. Trojano, B. Bielecki, M.P. Mycko, K. Selmaj, M. Santos, P. Maciel, C. Pereira,
662 A. Silva, B.M. Silva, F. Coraddu, M.G. Marrosu, E. Akesson, J. Hillert, P. Datta, A. Oturai,
663 H.F. Harbo, A. Spurkland, R. Goertsches, P. Villoslada, M. Eraksoy, A. Hensiek, A. Compston,
664 E. Setakis, J. Gray, T.W. Yeo, and S. Sawcer. 2006. Linkage disequilibrium screening for
665 multiple sclerosis implicates JAG1 and POU2AF1 as susceptibility genes in Europeans. *J*
666 *Neuroimmunol* 179:108-116.
667 Banerjee, A., S.M. Gordon, A.M. Intlekofer, M.A. Paley, E.C. Mooney, T. Lindsten, E.J. Wherry, and
668 S.L. Reiner. 2010. Cutting edge: The transcription factor eomesodermin enables CD8+ T cells
669 to compete for the memory cell niche. *J Immunol* 185:4988-4992.
670 Blattman, J.N., R. Antia, D.J. Sourdive, X. Wang, S.M. Kaech, K. Murali-Krishna, J.D. Altman, and
671 R. Ahmed. 2002. Estimating the precursor frequency of naive antigen-specific CD8 T cells. *J*
672 *Exp Med* 195:657-664.
673 Cafri, G., R. Yossef, A. Pasetto, D.C. Deniger, Y.C. Lu, M. Parkhurst, J.J. Gartner, L. Jia, S. Ray, L.T.
674 Ngo, M. Jafferji, A. Sachs, T. Prickett, P.F. Robbins, and S.A. Rosenberg. 2019. Memory T
675 cells targeting oncogenic mutations detected in peripheral blood of epithelial cancer patients.
676 *Nat Commun* 10:449.
677 Chevrier, S., T. Kratina, D. Emslie, A. Karnowski, and L.M. Corcoran. 2014. Germinal center-
678 independent, IgM-mediated autoimmunity in sanroque mice lacking Obf1. *Immunol Cell Biol*
679 92:12-19.
680 Crawford, A., J.M. Angelosanto, C. Kao, T.A. Doering, P.M. Odorizzi, B.E. Barnett, and E.J. Wherry.
681 2014. Molecular and transcriptional basis of CD4(+) T cell dysfunction during chronic
682 infection. *Immunity* 40:289-302.
683 Gearty, S.V., F. Dundar, P. Zumbo, G. Espinosa-Carrasco, M. Shakiba, F.J. Sanchez-Rivera, N.D.
684 Socci, P. Trivedi, S.W. Lowe, P. Lauer, N. Mohibullah, A. Viale, T.P. DiLorenzo, D. Betel,
685 and A. Schietinger. 2022. An autoimmune stem-like CD8 T cell population drives type 1
686 diabetes. *Nature* 602:156-161.
687 Hess Michelini, R., A.L. Doedens, A.W. Goldrath, and S.M. Hedrick. 2013. Differentiation of CD8
688 memory T cells depends on Foxo1. *J Exp Med* 210:1189-1200.
689 Ichii, H., A. Sakamoto, M. Arima, M. Hatano, Y. Kuroda, and T. Tokuhisa. 2007. Bcl6 is essential for
690 the generation of long-term memory CD4+ T cells. *Int Immunol* 19:427-433.
691 Joshi, N.S., W. Cui, A. Chandele, H.K. Lee, D.R. Urso, J. Hagman, L. Gapin, and S.M. Kaech. 2007.
692 Inflammation directs memory precursor and short-lived effector CD8(+) T cell fates via the
693 graded expression of T-bet transcription factor. *Immunity* 27:281-295.
694 Ju, S., Y. Zhu, L. Liu, S. Dai, C. Li, E. Chen, Y. He, X. Zhang, and B. Lu. 2009. Gadd45b and
695 Gadd45g are important for anti-tumor immune responses. *Eur J Immunol* 39:3010-3018.
696 Kallies, A., A. Xin, G.T. Belz, and S.L. Nutt. 2009. Blimp-1 transcription factor is required for the
697 differentiation of effector CD8(+) T cells and memory responses. *Immunity* 31:283-295.
698 Kim, C., D.C. Jay, and M.A. Williams. 2012. Stability and function of secondary Th1 memory cells
699 are dependent on the nature of the secondary stimulus. *J Immunol* 189:2348-2355.

700 Kim, H., J. Perovanovic, A. Shakya, Z. Shen, C.N. German, I. A., J.L. Jafek, N.-P. Lin, B.D. Evavold,
701 D.H. Chou, P.E. Jensen, X. He, and D. Tantin. 2021. Targeting OCA-B/Pou2af1 blocks
702 activated, autoreactive T cells in the pancreas and type-1 diabetes. *J Exp Med* 218:e20200533.
703 Lachmann, A., H. Xu, J. Krishnan, S.I. Berger, A.R. Mazloom, and A. Ma'ayan. 2010. ChEA:
704 transcription factor regulation inferred from integrating genome-wide ChIP-X experiments.
705 *Bioinformatics* 26:2438-2444.
706 Liu, L., E. Tran, Y. Zhao, Y. Huang, R. Flavell, and B. Lu. 2005. Gadd45 beta and Gadd45 gamma are
707 critical for regulating autoimmunity. *J Exp Med* 202:1341-1347.
708 Love, M.I., W. Huber, and S. Anders. 2014. Moderated estimation of fold change and dispersion for
709 RNA-seq data with DESeq2. *Genome Biol* 15:550.
710 Luo, Y., D.L. Boyle, D. Hammaker, M. Edgar, G. Franzoso, and G.S. Firestein. 2011. Suppression of
711 collagen-induced arthritis in growth arrest and DNA damage-inducible protein 45beta-deficient
712 mice. *Arthritis Rheum* 63:2949-2955.
713 Luo, Y., and R.G. Roeder. 1995. Cloning, functional characterization, and mechanism of action of the
714 B-cell-specific transcriptional coactivator OCA-B. *Mol. Cell. Biol.* 15:4115-4124.
715 Marshall, H.D., A. Chandele, Y.W. Jung, H. Meng, A.C. Poholek, I.A. Parish, R. Rutishauser, W. Cui,
716 S.H. Kleinstein, J. Craft, and S.M. Kaech. 2011. Differential expression of Ly6C and T-bet
717 distinguish effector and memory Th1 CD4(+) cell properties during viral infection. *Immunity*
718 35:633-646.
719 Mitchell, D.M., E.V. Ravkov, and M.A. Williams. 2010. Distinct roles for IL-2 and IL-15 in the
720 differentiation and survival of CD8+ effector and memory T cells. *J Immunol* 184:6719-6730.
721 Murali-Krishna, K., J.D. Altman, M. Suresh, D.J. Sourdive, A.J. Zajac, J.D. Miller, J. Slansky, and R.
722 Ahmed. 1998. Counting antigen-specific CD8 T cells: a reevaluation of bystander activation
723 during viral infection. *Immunity* 8:177-187.
724 Nakamura, M., N. Nishida, M. Kawashima, Y. Aiba, A. Tanaka, M. Yasunami, H. Nakamura, A.
725 Komori, M. Nakamuta, M. Zeniya, E. Hashimoto, H. Ohira, K. Yamamoto, M. Onji, S.
726 Kaneko, M. Honda, S. Yamagiwa, K. Nakao, T. Ichida, H. Takikawa, M. Seike, T. Umemura,
727 Y. Ueno, S. Sakisaka, K. Kikuchi, H. Ebinuma, N. Yamashiki, S. Tamura, Y. Sugawara, A.
728 Mori, S. Yagi, K. Shirabe, A. Taketomi, K. Arai, K. Monoe, T. Ichikawa, M. Taniai, Y.
729 Miyake, T. Kumagi, M. Abe, K. Yoshizawa, S. Joshita, S. Shimoda, K. Honda, H. Takahashi,
730 K. Hirano, Y. Takeyama, K. Harada, K. Migita, M. Ito, H. Yatsuhashi, N. Fukushima, H. Ota,
731 T. Komatsu, T. Saoshiro, J. Ishida, H. Kouno, H. Kouno, M. Yagura, M. Kobayashi, T. Muro,
732 N. Masaki, K. Hirata, Y. Watanabe, Y. Nakamura, M. Shimada, N. Hirashima, T. Komeda, K.
733 Sugi, M. Koga, K. Ario, E. Takesaki, Y. Maehara, S. Uemoto, N. Kokudo, H. Tsubouchi, M.
734 Mizokami, Y. Nakanuma, K. Tokunaga, and H. Ishibashi. 2012. Genome-wide association
735 study identifies TNFSF15 and POU2AF1 as susceptibility loci for primary biliary cirrhosis in
736 the Japanese population. *Am J Hum Genet* 91:721-728.
737 Oxenius, A., M.F. Bachmann, R.M. Zinkernagel, and H. Hengartner. 1998. Virus-specific MHC-class
738 II-restricted TCR-transgenic mice: effects on humoral and cellular immune responses after viral
739 infection. *Eur J Immunol* 28:390-400.
740 Pace, L., C. Goudot, E. Zueva, P. Gueguen, N. Burgdorf, J.J. Waterfall, J.P. Quivy, G. Almouzni, and
741 S. Amigorena. 2018. The epigenetic control of stemness in CD8(+) T cell fate commitment.
742 *Science* 359:177-186.
743 Pepper, M., A.J. Pagan, B.Z. Igyarto, J.J. Taylor, and M.K. Jenkins. 2011. Opposing signals from the
744 Bcl6 transcription factor and the interleukin-2 receptor generate T helper 1 central and effector
745 memory cells. *Immunity* 35:583-595.
746 Perovanovic, J., Y. Wu, H. Abewe, Z. Shen, E.P. Hughes, J. Gertz, M.B. Chandrasekharan, and D.
747 Tantin. 2023. Oct1 cooperates with the Smad family of transcription factors to promote
748 mesodermal lineage specification. *Sci. Signal.* 16:eadd5750.

749 Rao, R.R., Q. Li, M.R. Gubbels Bupp, and P.A. Shrikant. 2012. Transcription factor Foxo1 represses
750 T-bet-mediated effector functions and promotes memory CD8(+) T cell differentiation.
751 *Immunity* 36:374-387.
752 Rodriguez-Jimenez, P., L. Fernandez-Messina, M.C. Ovejero-Benito, P. Chicharro, P. Vera-Tome, A.
753 Vara, D. Cibrian, P. Martinez-Fleta, M. Jimenez-Fernandez, I. Sanchez-Garcia, M. Llamas-
754 Velasco, F. Abad-Santos, F. Sanchez-Madrid, E. Dauden, and H. de la Fuente. 2021. Growth
755 arrest and DNA damage-inducible proteins (GADD45) in psoriasis. *Sci Rep* 11:14579.
756 Rosato, P.C., S. Wijeyesinghe, J.M. Stolley, C.E. Nelson, R.L. Davis, L.S. Manlove, C.A. Pennell,
757 B.R. Blazar, C.C. Chen, M.A. Geller, V. Vezys, and D. Masopust. 2019. Virus-specific
758 memory T cells populate tumors and can be repurposed for tumor immunotherapy. *Nat*
759 *Commun* 10:567.
760 Rutishauser, R.L., G.A. Martins, S. Kalachikov, A. Chandele, I.A. Parish, E. Meffre, J. Jacob, K.
761 Calame, and S.M. Kaech. 2009. Transcriptional repressor Blimp-1 promotes CD8(+) T cell
762 terminal differentiation and represses the acquisition of central memory T cell properties.
763 *Immunity* 31:296-308.
764 Sallusto, F., A. Lanzavecchia, K. Araki, and R. Ahmed. 2010. From vaccines to memory and back.
765 *Immunity* 33:451-463.
766 Samardzic, T., D. Marinkovic, P.J. Nielsen, L. Nitschke, and T. Wirth. 2002. BOB.1/OBF.1 deficiency
767 affects marginal-zone B-cell compartment. *Mol Cell Biol* 22:8320-8331.
768 Sauter, P., and P. Matthias. 1997. The B cell-specific coactivator OBF-1 (OCA-B, Bob-1) is inducible
769 in T cells and its expression is dispensable for IL-2 gene induction. *Immunobiology* 198:207-
770 216.
771 Schnell, A., L. Huang, M. Singer, A. Singaraju, R.M. Barilla, B.M.L. Regan, A. Bollhagen, P.I.
772 Thakore, D. Dionne, T.M. Delorey, M. Pawlak, G. Meyer Zu Horste, O. Rozenblatt-Rosen,
773 R.A. Irizarry, A. Regev, and V.K. Kuchroo. 2021. Stem-like intestinal Th17 cells give rise to
774 pathogenic effector T cells during autoimmunity. *Cell* 184:6281-6298 e6223.
775 Shakya, A., A. Goren, A. Shalek, C.N. German, J. Snook, V.K. Kuchroo, N. Yosef, R.C. Chan, A.
776 Regev, M.A. Williams, and D. Tantin. 2015. Oct1 and OCA-B are selectively required for CD4
777 memory T cell function. *J Exp Med* 212:2115-2131.
778 Shakya, A., J. Kang, J. Chumley, M.A. Williams, and D. Tantin. 2011. Oct1 is a switchable,
779 bipotential stabilizer of repressed and inducible transcriptional states. *J Biol Chem* 286:450-
780 459.
781 Shen, H., M.K. Slifka, M. Matloubian, E.R. Jensen, R. Ahmed, and J.F. Miller. 1995. Recombinant
782 Listeria monocytogenes as a live vaccine vehicle for the induction of protective anti-viral cell-
783 mediated immunity. *Proc Natl Acad Sci U S A* 92:3987-3991.
784 Shin, H.M., V. Kapoor, T. Guan, S.M. Kaech, R.M. Welsh, and L.J. Berg. 2013. Epigenetic
785 modifications induced by Blimp-1 Regulate CD8(+) T cell memory progression during acute
786 virus infection. *Immunity* 39:661-675.
787 Snook, J.P., C. Kim, and M.A. Williams. 2018. TCR signal strength controls the differentiation of
788 CD4(+) effector and memory T cells. *Sci Immunol* 3:eaas9103.
789 Stuart, T., A. Butler, P. Hoffman, C. Hafemeister, E. Papalexi, W.M. Mauck, 3rd, Y. Hao, M.
790 Stoeckius, P. Smibert, and R. Satija. 2019. Comprehensive Integration of Single-Cell Data. *Cell*
791 177:1888-1902 e1821.
792 Utzschneider, D.T., M. Charmoy, V. Chennupati, L. Pousse, D.P. Ferreira, S. Calderon-Copete, M.
793 Danilo, F. Alfei, M. Hofmann, D. Wieland, S. Pradervand, R. Thimme, D. Zehn, and W. Held.
794 2016. T Cell Factor 1-Expressing Memory-like CD8(+) T Cells Sustain the Immune Response
795 to Chronic Viral Infections. *Immunity* 45:415-427.
796 Williams, M.A., E.V. Ravkov, and M.J. Bevan. 2008. Rapid culling of the CD4+ T cell repertoire in
797 the transition from effector to memory. *Immunity* 28:533-545.

798 Zwilling, S., A. Dieckmann, P. Pfisterer, P. Angel, and T. Wirth. 1997. Inducible expression and
799 phosphorylation of coactivator BOB.1/OBF.1 in T cells. *Science* 277:221-225.

Sun et al. Figure 1

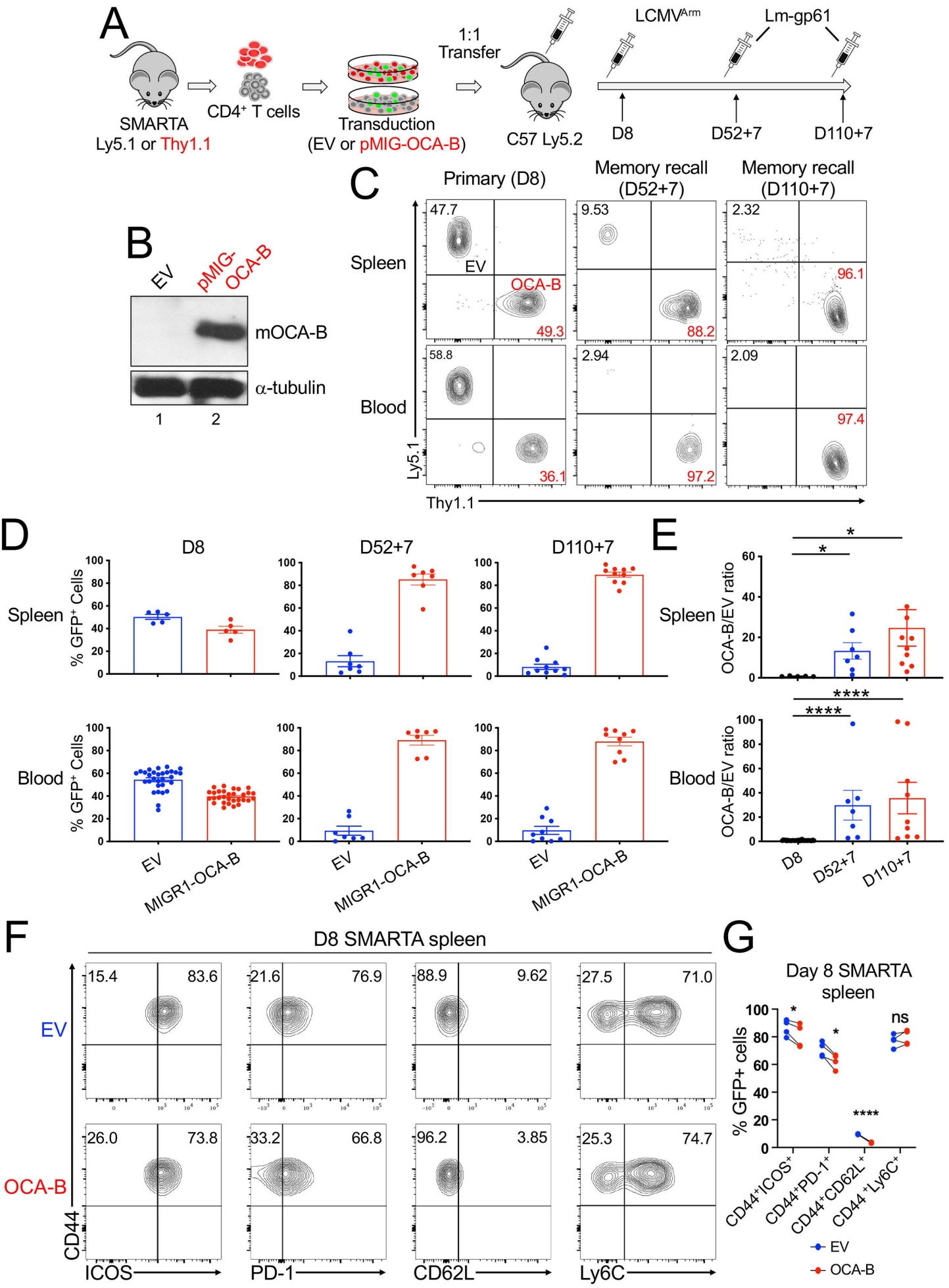

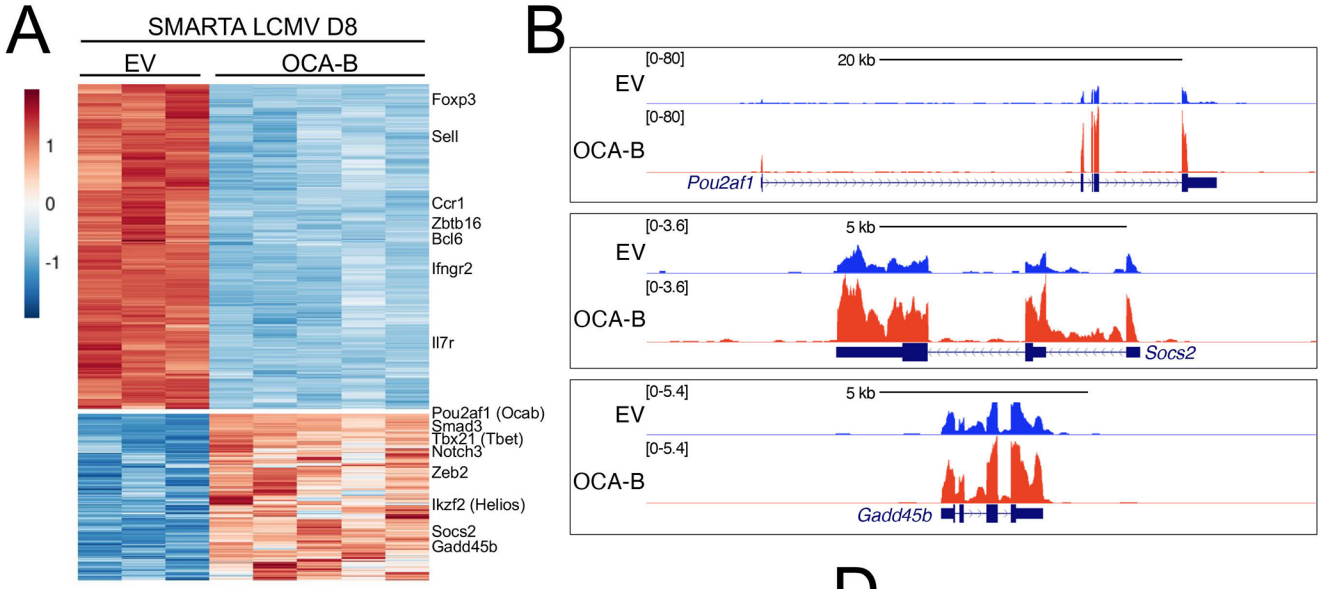

C

OCA-B upregulated genes

Epigenomic roadmap HM	*p*-value
H3K9me3 Breast vHMEC	0.048
Molecular function	***p*-value**
Toll-like receptor binding	0.006
Aspartic-type peptidase activity	0.007

OCA-B downregulated genes

Epigenomic roadmap HM	*p*-value
H3K27me3 CD4 Memory Primary Cells	1.45E-04
H3K27me3 CD8 Memory Primary Cells	9.30E-04
Molecular function	***p*-value**
Superoxide-generating NADPH oxidase activator activity	1.29E-09
Cytokine receptor activity	1.24E-06

D

OCA-B upregulated genes

ChEA 2016	*p*-value
Tp53	0.01936
Smc3	0.02544

OCA-B downregulated genes

ChEA 2016	*p*-value
IRF8	1.24E-20
SMRT	1.14E-15
MYB	1.73E-09
Nerf2	4.79E-09
NCOR	1.52E-08

Sun et al. Figure 3

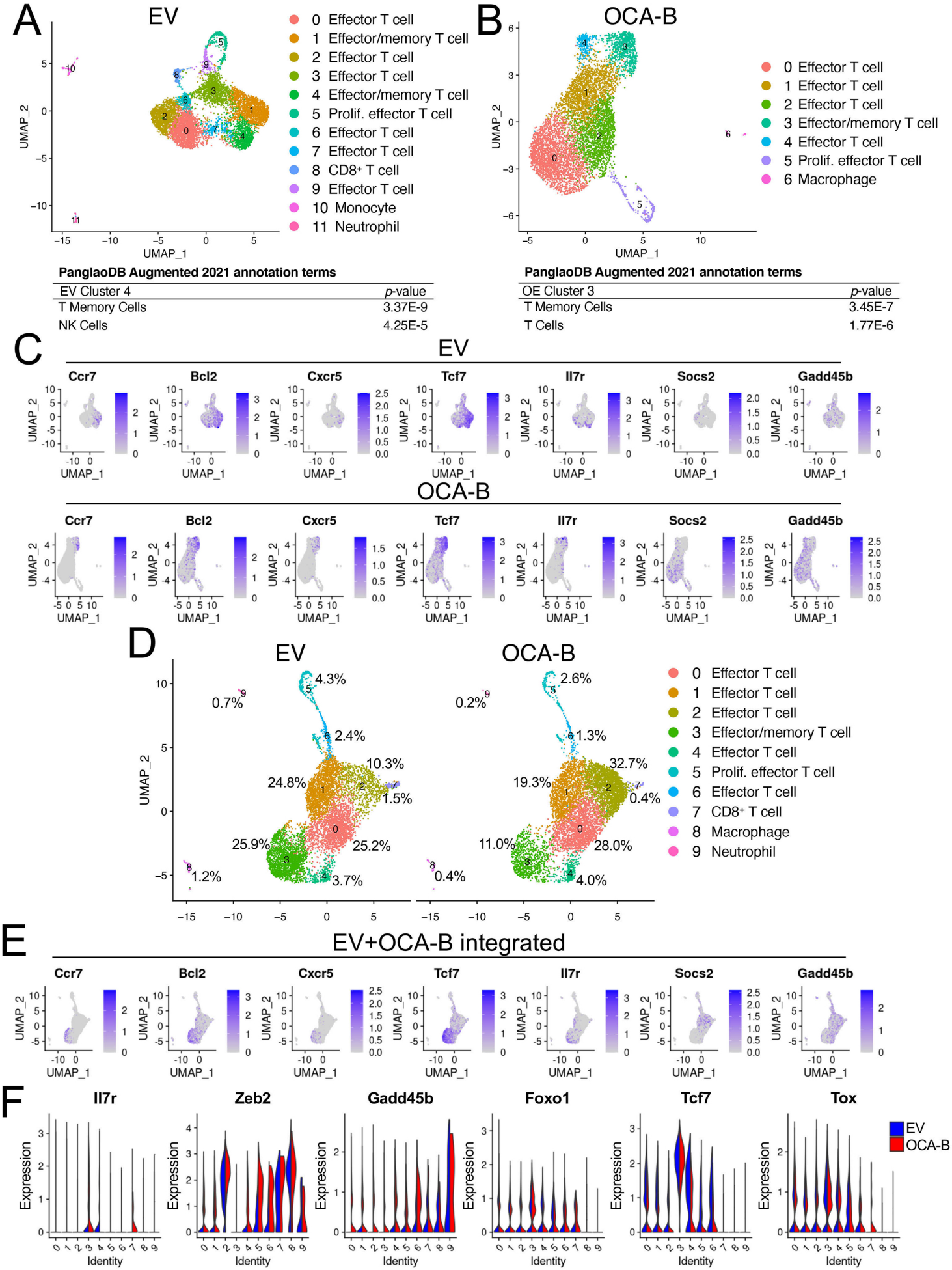

PanglaoDB Augmented 2021 annotation terms

EV Cluster 4	*p*-value
T Memory Cells	3.37E-9
NK Cells	4.25E-5

PanglaoDB Augmented 2021 annotation terms

OE Cluster 3	*p*-value
T Memory Cells	3.45E-7
T Cells	1.77E-6

Sun et al. Figure 4

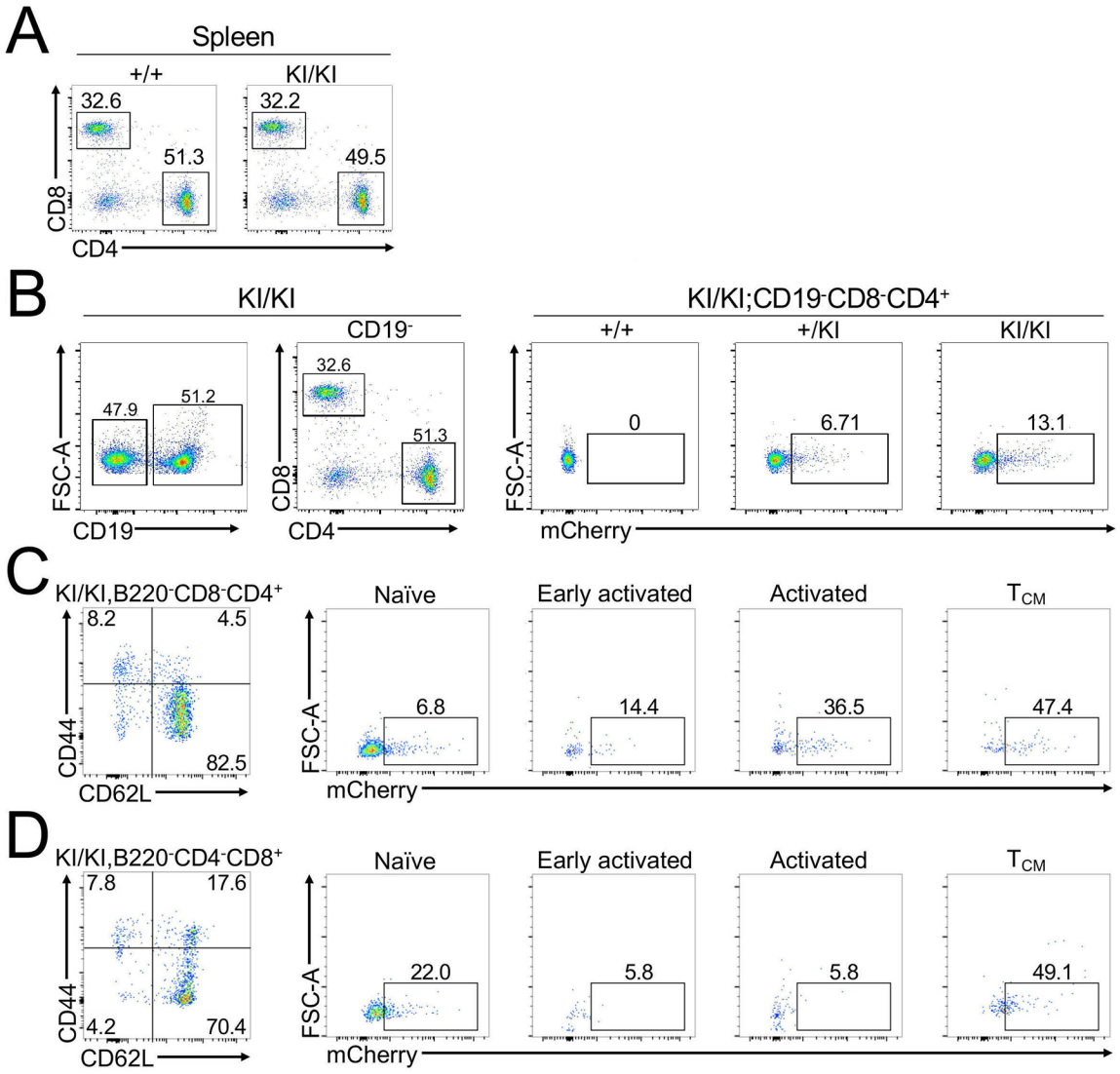
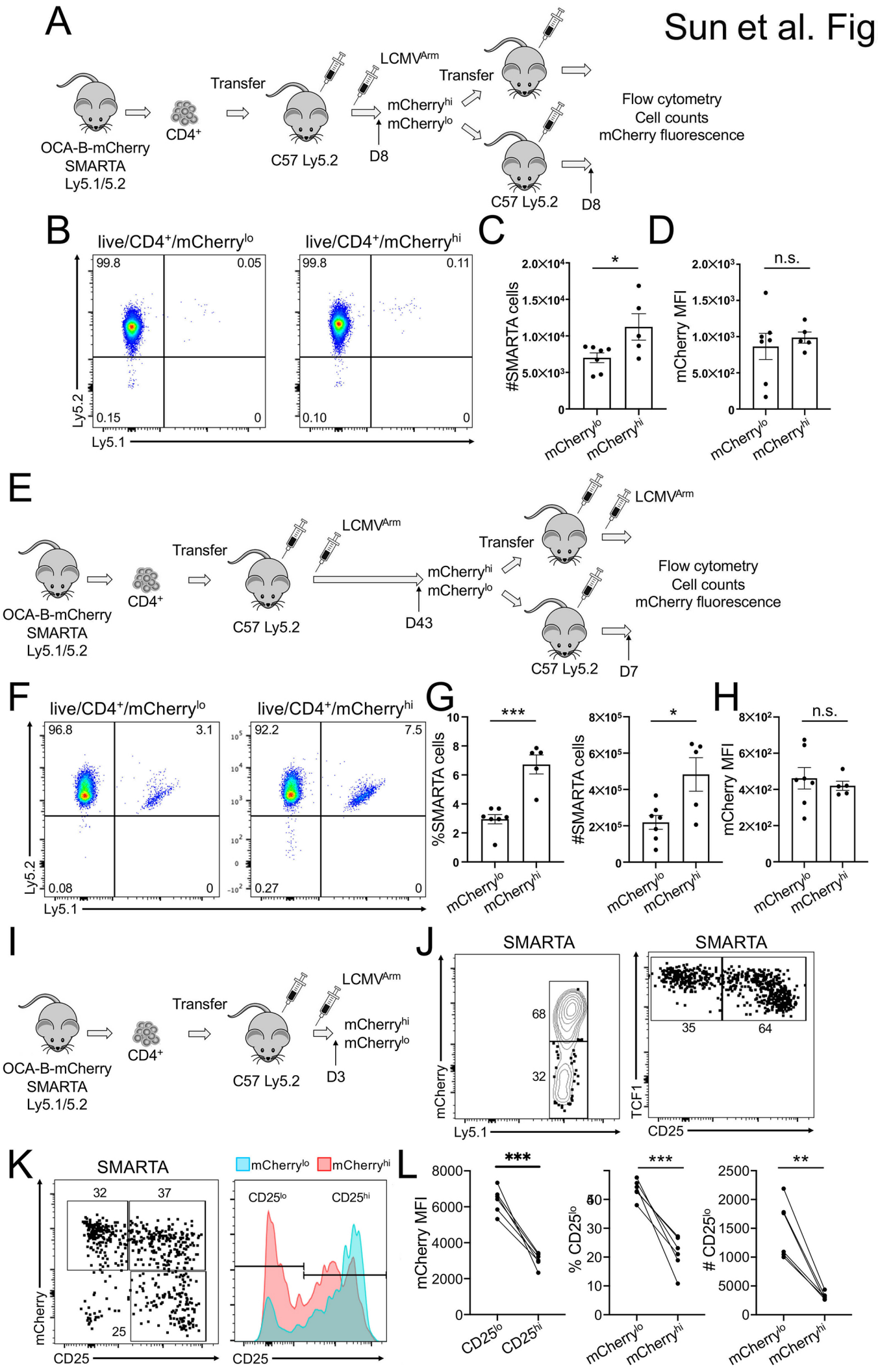
Sun et al. Figure 5